Origin of spectral hole burning in Brillouin fiber amplifiers and generators

L. Stépien, S. Randoux, and J. Zemmouri
Laboratoire de Physique des Lasers, Atomes et Molécules, UMR 8523, Centre d'Études et de Recherches Lasers et Applications, Université des Sciences et Technologies de Lille, F-59655 Villeneuve d'Ascq Cedex, France
(Received 5 October 2001; revised manuscript received 22 January 2002; published 3 May 2002)

We show theoretically that the spectral hole burning recently observed in Brillouin fiber amplifiers and generators can be interpreted without invoking an inhomogeneous broadening of the Brillouin line. By using the three-wave model of stimulated Brillouin scattering (SBS), we first investigate the linear response of a Brillouin fiber amplifier to a weak amplitude modulation of the injected signal wave. The transfer functions that fully characterize this response are analytically calculated. The fact that they may exhibit a dip is shown to be due both to the gain saturation and to the coupling between the pump and signal perturbations that counterpropagate around the steady-state intensity profiles. These transfer functions also appropriately characterize the way through which noisy perturbations are filtered in SBS fiber generators. The spectral hole burning observed in generators is thus simply connected to spectral hole burning studied in SBS amplifiers.

DOI: 10.1103/PhysRevA.65.053812 PACS number(s): 42.65.Es, 42.55.Wd, 42.81.−i

I. INTRODUCTION

Stimulated Brillouin scattering (SBS) is a nonlinear process that manifests through the generation of a backward-propagating Stokes wave whose frequency is down-shifted from that of the pump laser [1]. In optical fibers, two experimental configurations permit to study this interaction in a simple way: (i) the SBS generator and (ii) the SBS amplifier [2]. In the former configuration, great care is taken to avoid Fresnel reflections from the fiber ends and only one laser beam is injected into the fiber core. SBS is then initiated from thermally excited sound waves, and the intensity of the generated Stokes wave is found to exhibit fluctuations of a stochastic nature [3–5]. In the amplifier configuration, Fresnel reflections are also eliminated from the fiber ends but a strong pump field and a weak signal are now launched into the fiber. The signal is strongly amplified if its frequency falls within the Brillouin gain bandwidth that typically broadens up to several tens of megahertz [6]. The linewidth of the Stokes radiation delivered by Brillouin fiber generators is also of this order of magnitude [4]. This spectral broadening around the exact Stokes frequency arises from the finite response time ($\simeq 10$ ns) of the acoustic wave involved in the SBS interaction.

There is currently a lot of controversy about the exact nature of spectral broadening of SBS in optical fibers. Recent experiments performed both in a Brillouin fiber amplifier and in a Brillouin fiber generator have indeed revealed features that are usually observed as a laser radiation resonantly interacts with an atomic medium in which absorption lines are inhomogeneously broadened [7]. Actually, hole burning has been observed in the gain spectrum of a Brillouin fiber amplifier [8] and in the spectrum of intensity fluctuations of the Stokes light emitted by a Brillouin fiber generator [9]. As spectral hole burning usually typifies the interaction of laser radiation with an inhomogeneously broadened system, all the features experimentally observed have been attributed to an inhomogeneous broadening of the Brillouin line. According to Kovalev and Harrison who performed experiments in a Brillouin fiber generator [9], this inhomogeneous broadening arises from the waveguide interaction of the pump and Stokes waves. Following their interpretation, there is not only one Stokes frequency shift as should be the case if the SBS interaction involved plane waves. A continuum of frequency shifted Stokes components is generated because a single-mode fiber is able to guide a fan of beam directions within a small angle. However, this interpretation has been disputed by two of us [Randoux and Zemmouri (RZ)], having shown that the behaviors reported by Kovalev and Harrison can be simulated without invoking an inhomogeneous broadening of the Brillouin line [10]. In particular, RZ have shown that the hole burning presented in Ref. [9] can be reproduced by numerically integrating the equations of the usual three-wave model of SBS in, which both homogeneous broadening and plane-wave propagation are assumed. Similar numerical results have also been recently reported by Fotiadi *et al.* in Ref. [11]. In the Brillouin fiber amplifier, Takushima and Kikuchi have also shown that the occurrence of spectral gain hole burning can be described by using this three-wave model [12]. Nevertheless, some confusion now surrounds the nature of spectral broadening of SBS in optical fibers, partly because the physical mechanisms responsible for spectral hole burning of a homogeneously broadened Brillouin line remain unclear. Furthermore, no connection has been established between the spectral hole burning found in Brillouin fiber amplifiers and the spectral hole burning observed in Brillouin fiber generators.

The aim of this paper is to study theoretically the mechanisms inducing the emergence of spectral hole burning in a Brillouin line that is supposed to be homogeneously broadened. By using the three-wave model of SBS, we will show, in particular, that these mechanisms are identical both in the Brillouin fiber amplifier and in the Brillouin fiber generator. This paper is organized in the following way. The three-wave model of SBS is briefly presented in Sec. II. The origin of spectral gain hole burning in Brillouin fiber amplifiers is studied in Sec. III. In particular, we investigate the linear response of the Brillouin fiber amplifier to a weak amplitude modulation of the injected signal. Analytical expressions for the transfer functions that fully characterize this response are

determined for three different amplification regimes. The results obtained are then used in Sec. IV to explain the occurrence of hole burning in the spectrum of intensity fluctuations of Brillouin fiber generators. We thus show that the noisy perturbations propagating in generators are simply filtered by the transfer functions determined for the amplifier.

II. THE THREE-WAVE MODEL OF SBS

The theoretical study presented throughout this paper enters within the framework of the three-wave model of SBS, which is commonly used to describe the dynamics of Brillouin fiber lasers [13], amplifiers [14], and generators [4]. Let us recall that this model is derived by assuming that the nonlinear interaction does not alter the mode characteristics of the guide, so that the transverse evolution of the optical fields can be decoupled from their longitudinal one. As the SBS process is then supposed to involve infinite plane waves propagating collinearly along the fiber axis, the theoretical treatment is greatly simplified. In particular, this means that only one phase-matching relation is verified and that the mechanisms of inhomogeneous broadening by the guiding suggested in Ref. [9] cannot be described by using such an approach. The acoustic damping being supposed uniform in the fiber, the three-wave model of SBS is, furthermore, established by assuming that the Brillouin line is homogeneously broadened. Assuming linear polarization for the light beams and slowly varying envelopes for all the waves, neglecting the weak attenuation of the fiber and the perturbative optical Kerr effect, the dimensionless equations describing the SBS interaction read

$$\frac{\partial \varepsilon_p}{\partial \tau} + \frac{\partial \varepsilon_p}{\partial \zeta} = -gB\varepsilon_s, \tag{1a}$$

$$\frac{\partial \varepsilon_s}{\partial \tau} - \frac{\partial \varepsilon_s}{\partial \zeta} = gB^*\varepsilon_p, \tag{1b}$$

$$\frac{1}{\beta_A}\frac{\partial B}{\partial \tau} + B = \varepsilon_p \varepsilon_s^* + f(\zeta,\tau). \tag{1c}$$

ε_p, ε_s, and B represent, respectively, the complex envelopes of the pump, Stokes, and acoustic waves. The time τ is normalized to the transit time of the light inside the fiber. ζ is the space coordinate that is normalized to the fiber length L. The fields ε_p and ε_s are measured in units of the maximum pump field E_{max} available at the entrance end of the fiber. g is the normalized SBS coupling constant. β_A, which represents the normalized damping rate of the acoustic wave, is equal to $\pi \Delta\nu_B nL/c$, where c/n and $\Delta\nu_B$ are the phase velocity of light inside the fiber and the Brillouin spontaneous linewidth, respectively. Full details concerning the adopted normalization are given in Ref. [15].

$f(\zeta,\tau)$ is a weak noise term describing the random thermal fluctuations of density occurring inside the fiber. As it represents spontaneous scattering, its relative importance is much weaker than that of the term $\varepsilon_p\varepsilon_s^*$ associated with stimulated Brillouin scattering. However, its influence cannot be neglected in Brillouin fiber generators, in which the stochastic fluctuations of the Stokes intensity are completely shaped by the randomness of spontaneous scattering [3,4]. In Brillouin fiber amplifiers, two counterpropagating laser fields are launched into the fiber, and the dynamics no longer remains noise dominated but becomes purely deterministic [14]. In typical experiments, Brillouin amplifiers operate in a stable fixed state in which the signal wave is strongly and monotonically amplified [6]. The influence of the noise term $f(\zeta,\tau)$ is then commonly fully neglected [12,16].

The normalized parameters used throughout this paper are $g=10.98$ and $\beta_A=18.22$. They are computed from SBS coupling constants commonly found in the literature [15,17] and from physical values corresponding to typical optical-fiber experiments. The fiber length is supposed to be 60 m and its core diameter is equal to 8 μm. At a pumping wavelength of 1550 nm, $\Delta\nu_B$ is estimated to be 20 MHz [6]. The maximum pump field E_{max} chosen for the normalization is 2.27 MV/m and corresponds to an injected pump power of 500 mW. To clearly precise the relation between our reduced variables and physically measurable quantities, a normalized pump intensity $|\varepsilon_p(\zeta=0)|^2$ equal to unity corresponds to a pump power of 500 mW injected inside the fiber core. A normalized time variation of unity corresponds to 0.29 μs and a normalized angular frequency ω of 2π corresponds to a physical angular frequency of $2\pi\times 3.4\times 10^6$ rad/s.

III. SPECTRAL GAIN HOLE BURNING IN BRILLOUIN FIBER AMPLIFIERS

The aim of this section is to study the mechanisms responsible for the emergence of hole burning in the gain bandwidth of Brillouin fiber amplifiers. In Sec. III A, we first recall the approach adopted in Ref. [12] by Takushima and Kikuchi who have proposed a configuration in which spectral hole burning is evidenced by injecting three optical waves into a Brillouin fiber amplifier. After a brief discussion about the relation between this approach and pump-probe studies performed in atomic systems, we show that this three-wave configuration is equivalent to a two-wave configuration in which the amplitude of the signal wave is weakly modulated. This permits to greatly simplify the theoretical treatment, since only the equations governing the evolution of the field amplitudes have to be considered. These amplitude equations are linearized and the problem is reduced to the determination of transfer functions characterizing the way through which the amplitude modulation is filtered by the amplifier. These transfer functions fully characterize the linear response of the amplifier and they are analytically calculated for three different regimes ranging from unsaturated to saturated amplification. By using appropriate approximated expressions for the stationary pump and signal intensity profiles, Sec. III B, III C, and III D are thus devoted to the theoretical treatment of the weak interaction, the weak saturation, and the strong saturation regimes, respectively.

A. Theoretical approach and approximations

In Ref. [12], Takushima and Kikuchi consider that the Brillouin amplifier operates in a stable fixed state obtained

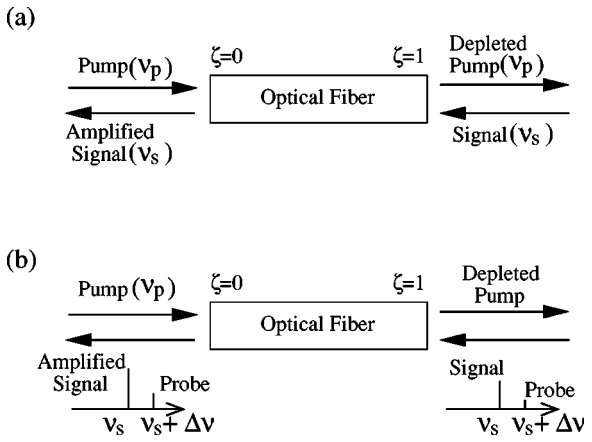

FIG. 1. Two possible configurations for studying Brillouin fiber amplifiers. (a) Usual two-wave configuration studied in Ref. [14]. (b) Three-wave configuration studied in Ref. [12].

by injecting two counterpropagating laser beams into the fiber [see Fig. 1(a)]. A strong pump field (weak signal field) oscillating at an optical frequency ν_p (ν_s) is launched into the fiber at $\zeta=0$ ($\zeta=1$). The frequency detuning $\nu_p-\nu_s$ between the two fields is equal to the Brillouin shift in silica so that the signal is strongly and resonantly amplified. Additionally, a probe field oscillating at a frequency $\nu_s+\Delta\nu$ is launched in the fiber at $\zeta=1$ [see Fig. 1(b)]. Whatever ζ, the amplitude $a_{pr}(\zeta)$ of this field is much weaker than that of the pump and signal fields. The gain $G_{pr}=a_{pr}(\zeta=0)/a_{pr}(\zeta=1)$ experienced by the probe in the amplifier is then measured as a function of $\Delta\nu$. If the intensity of the signal wave is sufficiently low, the gain of the amplifier is not saturated and a bell-shaped curve is recorded. On the other hand, the function $G_{pr}(\Delta\nu)$ is found to exhibit a dip around $\Delta\nu\simeq 0$ as gain saturation is reached. The theoretical analysis performed by Takushima and Kikuchi enters within the framework of the three-wave model presented in Sec. II. Equations (1) are linearized by assuming that the probe field generates weak perturbations that propagate around the stationary profiles of the pump and signal fields. This leads to four differential equations governing the longitudinal evolution of the complex amplitudes of various sidebands oscillating at $\pm\Delta\nu$. Finally, these equations are numerically integrated and the function $G_{pr}(\Delta\nu)$ is plotted for increasing values of the signal intensity.

The approach adopted by Takushima and Kikuchi is quite analogous to that used in pump-probe studies performed in atomic systems. In standard pump-probe experiments, the pump beam ''prepares'' the atomic system, which is subsequently monitored by the probe beam. In Refs. [12,8], the pump and signal beams ''prepare'' the Brillouin fiber amplifier in a stationary state, which is subsequently monitored by the probe beam. In inhomogeneously broadened atomic systems, it is well known that a dip is observed in the probe absorption profile as the pump beam saturates one segment of the absorption line. However, the emergence of spectral hole burning at the frequency of the pump laser must not be interpreted straightforwardly as being a signature of an inhomogeneous broadening of the absorption line. The presence of a strong wave may indeed cause the absorption line to appear to be ''hole burned'' when probed by a second wave, even though the broadening mechanisms are homogeneous [18]. This phenomenon has been studied in the 1980s. It arises from a periodic modulation of the ground-state population at the beat frequency between the pump and probe fields [19,20]. From this brief summary of spectral hole burning in atomic systems, it appears that the mechanisms responsible for the emergence of a dip in the Brillouin gain spectrum may be subtle and that no simple conclusion can be drawn straightforwardly from the observation of such a phenomenon.

After this qualitative discussion, let us now examine how the theoretical treatment of spectral hole burning in Brillouin fiber amplifiers can be further developed. To describe the behavior of the Brillouin fiber amplifier represented in Fig. 1(b), Eqs. (1) must be completed by the following boundary conditions:

$$\varepsilon_p(\zeta=0,\tau)=\mu, \tag{2a}$$

$$\varepsilon_s(\zeta=1,\tau)=a_s(1+\alpha e^{i\Delta\Omega\tau}). \tag{2b}$$

μ is a dimensionless pump parameter and a_s represents the amplitude of the signal field injected into the amplifier. α is a small dimensionless parameter determining the ratio between the probe and signal amplitudes ($\alpha=a_{pr}/a_s\simeq 10^{-3}$). $\Delta\Omega$ is proportional to the frequency detuning between the signal and the probe fields ($\Delta\Omega=2\pi\Delta\nu nL/c$). By considering that $\alpha\ll 1$, the intensity $I_s(\zeta=1,\tau)$ and the phase $\phi_s(\zeta=1,\tau)$ of the complex field $\varepsilon_s(\zeta=1,\tau)$ can be easily determined and read,

$$I_s(\zeta=1,\tau)=|\varepsilon_s(\zeta=1,\tau)|^2\simeq a_s^2[1+2\alpha\cos(\Delta\Omega\tau)], \tag{3a}$$

$$\tan[\phi_s(\zeta=1,\tau)]\simeq\alpha\sin(\Delta\Omega\tau). \tag{3b}$$

These expressions show that adding a weak probe field that is frequency detuned to a resonant signal field is equivalent to weakly modulating both the amplitude and the phase of the signal wave. Let us now examine how this simple result can be used to simplify the theoretical analysis, and let us first transform the complex variables of Eqs. (1) to modulus-phase form. By neglecting the noise term $f(\zeta,\tau)$ of Eq. (1c), we obtain

$$\frac{\partial A_p}{\partial\tau}+\frac{\partial A_p}{\partial\zeta}=-gA_aA_s\cos\theta, \tag{4a}$$

$$\frac{\partial A_s}{\partial\tau}-\frac{\partial A_s}{\partial\zeta}=gA_aA_p\cos\theta, \tag{4b}$$

$$\frac{1}{\beta_A}\frac{\partial A_a}{\partial\tau}+A_a=A_pA_s\cos\theta, \tag{4c}$$

$$\frac{\partial\phi_p}{\partial\tau}+\frac{\partial\phi_p}{\partial\zeta}=-g\frac{A_aA_s}{A_p}\sin\theta, \tag{4d}$$

$$\frac{\partial \phi_s}{\partial \tau} - \frac{\partial \phi_s}{\partial \zeta} = -g \frac{A_a A_p}{A_s} \sin\theta, \tag{4e}$$

$$\frac{1}{\beta_A} \frac{\partial \phi_a}{\partial \tau} = -\frac{A_p A_s}{A_a} \sin\theta, \tag{4f}$$

where A_i and ϕ_i $(i=p,s,a)$ represent, respectively, the amplitudes and phases of the pump, Stokes, and acoustic waves. The variable $\theta(\zeta,\tau)$ is a function of the phases, which is equal to $\phi_s(\zeta,\tau)+\phi_a(\zeta,\tau)-\phi_p(\zeta,\tau)$. The amplitude and the phase of the signal wave at $\zeta=1$ being weakly modulated, one can consider that the amplitudes and the phases of all the waves involved in the SBS interaction will weakly fluctuate around their steady state. In these conditions, solutions of Eqs. (4) can be sought under the following form:

$$A_i(\zeta,\tau) = A_i^0(\zeta) + \delta A_i(\zeta,\tau) \quad (i=p,s,a), \tag{5a}$$

$$\phi_i(\zeta,\tau) = \phi_i^0(\zeta) + \delta\phi_i(\zeta,\tau) \quad (i=p,s,a). \tag{5b}$$

The functions $A_i^0(\zeta)$ $[\phi_i^0(\zeta)]$ are the steady-state profiles of the field amplitudes [phases] calculated in Ref. [14]. The functions $\delta A_i(\zeta,\tau)$ $[\delta\phi_i(\zeta,\tau)]$ represent the slight deviations of these amplitudes [phases] from their steady-state profiles. If the frequency of the signal wave is precisely tuned to the center of the Brillouin gain bandwidth, all the stationary phase profiles $\phi_i^0(\zeta)$ are uniformly equal to zero [14] and the variable $\theta(\zeta,\tau)$ then slightly fluctuates around zero. The term $\cos\theta$ present in Eqs. (4a)–(4c) only brings second-order terms that are neglected when the linearization is performed by substituting Eqs. (5) into Eqs. (4). To the first order, amplitude fluctuations are thus decoupled from phase fluctuations. As we are mainly interested in determining the gain experienced by the probe wave, we will ignore the phase equations and only consider the equations governing the spatiotemporal evolution of the amplitude fluctuations.

By introducing relative amplitude fluctuations defined as $\widetilde{\delta A}_i(\zeta,\tau) = \delta A_i(\zeta,\tau)/A_i^0(\zeta)$, we obtain

$$\frac{\partial \widetilde{\delta A}_p}{\partial \tau} + \frac{\partial \widetilde{\delta A}_p}{\partial \zeta} = g I_s(\zeta)(\widetilde{\delta A}_p - \widetilde{\delta A}_a - \widetilde{\delta A}_s), \tag{6a}$$

$$\frac{\partial \widetilde{\delta A}_s}{\partial \tau} - \frac{\partial \widetilde{\delta A}_s}{\partial \zeta} = g I_p(\zeta)(\widetilde{\delta A}_p + \widetilde{\delta A}_a - \widetilde{\delta A}_s), \tag{6b}$$

$$\frac{1}{\beta_A} \frac{\partial \widetilde{\delta A}_a}{\partial \tau} = \widetilde{\delta A}_p + \widetilde{\delta A}_s - \widetilde{\delta A}_a, \tag{6c}$$

where the functions $I_i(\zeta)=[A_i^0(\zeta)]^2$ $(i=p,s)$ represent the steady-state intensity profiles of the pump and signal waves inside the Brillouin fiber amplifier. These equations must be completed by boundary conditions, expressing that the amplitude of the pump laser is constant whereas the amplitude of the signal field is sinusoidally modulated. They read

$$\widetilde{\delta A}_p(\zeta=0,\tau) = 0, \tag{7a}$$

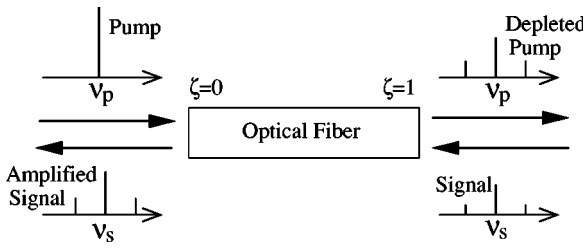

FIG. 2. Schematic representation of a Brillouin fiber amplifier submitted to a weak amplitude modulation of the signal. This configuration is equivalent to that presented in Fig. 1(b).

$$\widetilde{\delta A}_s(\zeta=1,\tau) = \alpha \cos(\Delta\Omega\,\tau). \tag{7b}$$

With these boundary conditions, the spectra of the various fields at the input and output ends of the fiber consist of carriers and weak sidebands. This is schematically represented in Fig. 2, which shows the spectral components involved in a Brillouin fiber amplifier submitted to a weak amplitude modulation of the injected signal wave. Let us emphasize that this configuration is equivalent to that studied by Takushima and Kikuchi in Ref. [12] [see also Fig. 1(b)]. However, it should be noted that Takushima and Kikuchi directly linearize the set of Eqs. (1) to obtain a set of four complex differential equations, which is solved only numerically. On the other hand, our theoretical treatment can now be further developed and, as shown hereafter, analytical solutions can be found from the unsatured to the saturated amplification regimes.

The next step of our theoretical analysis consists in taking the Fourier transforms of Eqs. (6). We then obtain two coupled differential equations governing the spatial evolutions of the Fourier transforms $\widetilde{\delta A}_p(\zeta,\omega)$ and $\widetilde{\delta A}_s(\zeta,\omega)$ of the functions $\widetilde{\delta A}_p(\zeta,\tau)$ and $\widetilde{\delta A}_s(\zeta,\tau)$. They read

$$\frac{\partial \widetilde{\delta A}_s(\zeta,\omega)}{\partial \zeta} = i\omega\left(\frac{g I_p(\zeta)}{\beta_A + i\omega} + 1\right)\widetilde{\delta A}_s(\zeta,\omega) - g I_p(\zeta)\left(1 + \frac{\beta_A}{\beta_A + i\omega}\right)\widetilde{\delta A}_p(\zeta,\omega), \tag{8a}$$

$$\frac{\partial \widetilde{\delta A}_p(\zeta,\omega)}{\partial \zeta} = -g I_s(\zeta)\left(1 + \frac{\beta_A}{\beta_A + i\omega}\right)\widetilde{\delta A}_s(\zeta,\omega) + i\omega\left(\frac{g I_s(\zeta)}{\beta_A + i\omega} - 1\right)\widetilde{\delta A}_p(\zeta,\omega). \tag{8b}$$

With our normalization, the steady-state intensity profiles of the pump and signal waves calculated in Ref. [14] read

$$I_p(\zeta) = \frac{I_p(0)(1-r)}{1 - r\exp(-\gamma\zeta)}, \tag{9a}$$

$$I_s(\zeta) = \frac{I_p(0) r (1-r)}{\exp(\gamma\zeta) - r} \tag{9b}$$

with

$$r=\frac{I_s(0)}{I_p(0)}, \tag{10a}$$

$$\gamma=2gI_p(0)(1-r). \tag{10b}$$

For small values of the parameter r (i.e., $r<10^{-4}$), the amplifier operates in the weak-interaction regime. Pump depletion can be ignored and the signal wave is exponentially amplified. In other words, the stationary pump and signal profiles can be approximated to

$$I_p(\zeta)=I_p(0), \tag{11a}$$

$$I_s(\zeta)=rI_p(0)\exp(-\gamma\zeta) \tag{11b}$$

with $\gamma=2gI_p(0)$. For values of r ranging approximately between 10^{-2} and 10^{-3}, the Brillouin fiber amplifier operates in the weak saturation regime. Pump depletion is then not very pronounced and it can be ignored. Equations (11) are still adequate but γ can no longer be approximated to $2gI_p(0)$, and Eq. (10b) must be used to describe the weak gain reduction that occurs in this regime. For values of r between 10^{-2} and 1, the amplifier operates in the strong saturation regime in which pump depletion cannot be ignored. For moderate values of r (i.e., $r<0.1$), an approximate expression of the pump intensity profile can be found by expanding Eq. (9a) to the first order in r. It reads

$$I_p(\zeta)=I_p(0)\{1-r[1-\exp(-\gamma\zeta)]\}. \tag{12}$$

It can be easily seen that the exponential term of Eq. (12) does not play an important role for values of ζ greater than $1/\gamma\simeq 0.1$. The signal amplification thus remains nearly exponential even in the strong saturation regime. As long as r does not exceed 0.1, Eqs. (11b) and (12), therefore, describe intensity profiles that are very close to the exact solutions given by Eqs. (9). By using the approximated intensity profiles given above, Secs. III B, III C, and III D are devoted to the analytical resolution of the set of Eqs. (8) in the weak-interaction, weak saturation and strong saturation, regimes, respectively.

B. Weak-interaction regime

By using Eqs. (11), the set of Eqs. (8) is first transformed into a second-order differential equation that reads

$$\frac{\partial^2\widetilde{\delta A}_s(\zeta,\omega)}{\partial\zeta^2}+2(\Gamma_0+\Gamma_1e^{-\gamma\zeta})\frac{\partial\widetilde{\delta A}_s(\zeta,\omega)}{\partial\zeta}+[\omega^2+2i\omega(\Gamma_0-\Gamma_1e^{-\gamma\zeta})+\Omega_1^2e^{-\gamma\zeta}]\widetilde{\delta A}_s(\zeta,\omega)=0 \tag{13}$$

with

$$\Gamma_0=\frac{-i\omega gI_p(0)}{2(\beta_A+i\omega)},\quad \Gamma_1=\frac{-i\omega gI_s(0)}{2(\beta_A+i\omega)},$$

and

$$\Omega_1^2=\frac{-4\beta_Ag^2I_p(0)I_s(0)}{\beta_A+i\omega}. \tag{14}$$

In the weak-interaction regime, the signal intensity is so weak that the problem can be examined to the lowest order in $I_s(0)$. The coefficients Γ_1 and Ω_1^2 are thus considered as being equal to zero and Eq. (13) then simply becomes

$$\frac{\partial^2\widetilde{\delta A}_s(\zeta,\omega)}{\partial\zeta^2}+2\Gamma_0\frac{\partial\widetilde{\delta A}_s(\zeta,\omega)}{\partial\zeta}+\Omega_0^2\widetilde{\delta A}_s(\zeta,\omega)=0 \tag{15}$$

with

$$\Omega_0^2=\omega^2\left(1+\frac{gI_p(0)}{\beta_A+i\omega}\right). \tag{16}$$

Taking the spatial Fourier transform of Eq. (15), we obtain a polynomial equation of degree 2 for the wave number k characterizing the propagation of the perturbation $\widetilde{\delta A}_s$ inside the amplifier. The two roots of the polynomial provide two dispersion relations that read

$$k_1=\omega\left(1+\frac{gI_p(0)}{\beta_A+i\omega}\right), \tag{17a}$$

$$k_2=-\omega. \tag{17b}$$

The solution of Eq. (15) can then simply be written as

$$\widetilde{\delta A}_s(\zeta,\omega)=C_1\exp(ik_1\zeta)+C_2\exp(ik_2\zeta), \tag{18}$$

where C_1 and C_2 are integration constants that must be determined from the boundary conditions. In particular, the combination of Eq. (7a) with Eq. (8a) permits to obtain a condition showing that C_2 is equal to zero. Taking into account this last result and substituting Eq. (18) into Eq. (8a) yields $\widetilde{\delta A}_p(\zeta,\omega)=0$. Therefore, in the weak-interaction regime, the pump wave is much stronger than the signal wave and it remains unaffected by the amplitude modulation applied to the signal at $\zeta=1$. Moreover, it is worth noticing that the propagation of the signal perturbation is supported by only one of the two possible wave vectors ($C_2=0$). The gain experienced by a signal perturbation oscillating at an angular frequency ω can thus be directly determined from the imaginary part of k_1 and it simply reads

$$|G_0(\omega)|=\left|\frac{\widetilde{\delta A}_s(\zeta=0,\omega)}{\widetilde{\delta A}_s(\zeta=1,\omega)}\right|=\exp\left(\frac{-gI_p(0)\omega^2}{\beta_A^2+\omega^2}\right). \tag{19}$$

The function $|G_0(\omega)|$ is plotted in Fig. 3(a) and its analytical expression can be directly connected to the usual expression of the gain of a Brillouin amplifier [2,12]. When pump depletion is ignored, the gain $G_{Ampli}(\omega)$ experienced by a signal wave that is detuned by ω from the center of the Brillouin bandwidth indeed reads

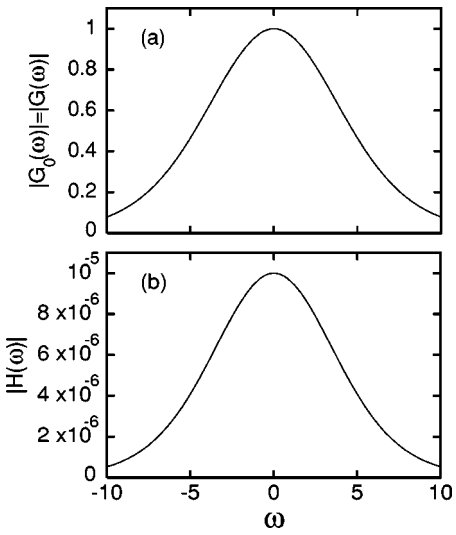

FIG. 3. Transfer functions characterizing the linear response of the Brillouin fiber amplifier in the weak-interaction regime. The parameters used are $g=10.98$, $\beta_A=18.22$, $I_p(0)=1$, $r=10^{-5}$.

$$G_{Ampli}(\omega)=\frac{I_s(\zeta=0)}{I_s(\zeta=1)}=\exp\left(\frac{2gI_p(0)\beta_A^2}{\beta_A^2+\omega^2}\right). \tag{20}$$

Normalizing this last expression with respect to the maximum gain, $\exp[2gI_p(0)]$, and taking the square root of the obtained result simply leads to Eq. (19). This means that all the configurations presented in Figs. 1 and 2 provide results that are qualitatively analogous about the gain bandwidth in the weak-interaction regime.

C. Weak saturation regime

In the weak saturation regime, the parameter r is approximately between 10^{-3} and 10^{-2}. In these conditions, Γ_1 can still be neglected with respect to Γ_0 in Eq. (13). On the other hand, the term Ω_1^2 clearly plays a role that cannot be ignored for values of ω that are sufficiently low [see expressions (14) and the third term of the left-hand side of Eq. (13)]. These considerations being taken into account, our working equation becomes

$$\frac{\partial^2\widetilde{\delta A}_s(\zeta,\omega)}{\partial\zeta^2}+2\Gamma_0\frac{\partial\widetilde{\delta A}_s(\zeta,\omega)}{\partial\zeta}+(\Omega_0^2+\Omega_1^2e^{-\gamma\zeta})\widetilde{\delta A}_s(\zeta,\omega)=0. \tag{21}$$

One of the coefficients of Eq. (21) being a function of ζ, the treatment already performed for Eq. (15) cannot be applied. In particular, it is not possible to derive two dispersion relations for the propagation of the signal perturbation. Nevertheless, the solution of Eq. (21) can be found by introducing the new variable $u=\exp(-\gamma\zeta)$. This yields the equation

$$\gamma^2u^2\frac{\partial^2\widetilde{\delta A}_s(u,\omega)}{\partial u^2}+\gamma u(\gamma-2\Gamma_0)\frac{\partial\widetilde{\delta A}_s(u,\omega)}{\partial u}+(\Omega_0^2+\Omega_1^2u)\widetilde{\delta A}_s(u,\omega)=0, \tag{22}$$

which admits the solution

$$\widetilde{\delta A}_s(u,\omega)=[C_1'J_A(B\sqrt{u})+C_2'Y_A(B\sqrt{u})]u^{\Gamma_0/\gamma}, \tag{23}$$

where $J_A(B\sqrt{u})$ and $Y_A(B\sqrt{u})$ are Bessel functions of the first and second kinds, respectively [21]. The coefficients A and B are given by

$$A=\frac{2\sqrt{\Gamma_0^2-\Omega_0^2}}{\gamma}\quad\text{and}\quad B=\frac{2\Omega_1}{\gamma}. \tag{24}$$

The integration constants C_1' and C_2' must be determined from the boundary conditions. From their expressions, it is, in particular, possible to derive the analytical expressions of two transfer functions $|G(\omega)|$ and $|H(\omega)|$ defined as

$$|G(\omega)|=\left|\frac{\widetilde{\delta A}_s(\zeta=0,\omega)}{\widetilde{\delta A}_s(\zeta=1,\omega)}\right|\quad\text{and}\quad|H(\omega)|=\left|\frac{\widetilde{\delta A}_p(\zeta=1,\omega)}{\widetilde{\delta A}_s(\zeta=1,\omega)}\right|. \tag{25}$$

$|G(\omega)|$ [$|H(\omega)|$] relates the amplitude fluctuations of the signal at $\zeta=0$ [the pump at $\zeta=1$] to the amplitude fluctuations of the signal applied at $\zeta=1$. Their analytical forms involve complicated combinations of Bessel functions that are given in Appendix A.

Let us now discuss the modifications affecting the functions $|G(\omega)|$ and $|H(\omega)|$ as r increases. First of all, it is worth noticing that there is no significant difference between $|G(\omega)|$ and $|G_0(\omega)|$ when the Stokes intensity $I_s(0)$ is much weaker than the pump intensity $I_p(0)$. This is illustrated in Fig. 3(a) which shows that the two functions are identical in the weak-interaction regime for $r=10^{-5}$. The analytical forms of $|G_0(\omega)|$ and $|G(\omega)|$ differ because they are not built from the same basis functions. The approach used to obtain the expression of $|G_0(\omega)|$ is indeed very simple and permits to obtain a solution that reads as a linear combination of exponential functions [Eq. (18)]. This means that the propagation modes authorized for the signal perturbation inside the amplifier are progressive sine waves that are exponentially damped. As the boundary condition for the pump wave [Eq. (7a)] imposes that only one of these propagation modes is excited, the gain $|G_0(\omega)|$ experienced by the signal perturbation is the simple exponential function given by Eq. (19). On the other hand, the approach leading to the analytical expression of $|G(\omega)|$ [Eq. (A2)] is much less restrictive than the previous one. The solution is also much more complicated and reads as a linear combination of Bessel functions [Eq. (23)]. This means that the propagation of the signal perturbation inside the amplifier still involves two propagation modes, but they do not remain simple progressive sine waves. Moreover, it should be noted that both of them are excited even in the weak-interaction regime ($C_1'\neq C_2'\neq 0$). Figure 3(b) shows that $|H(\omega)|$ is a bell-shaped function characterized by a peak value that is very small ($\simeq r=10^{-5}$) in the weak-interaction regime. This means that the signal fluctuation propagates inside the amplifier without significantly perturbating the pump amplitude. This result was also found in Sec. III B by treating Eq. (13) to the lowest order in $I_s(0)$.

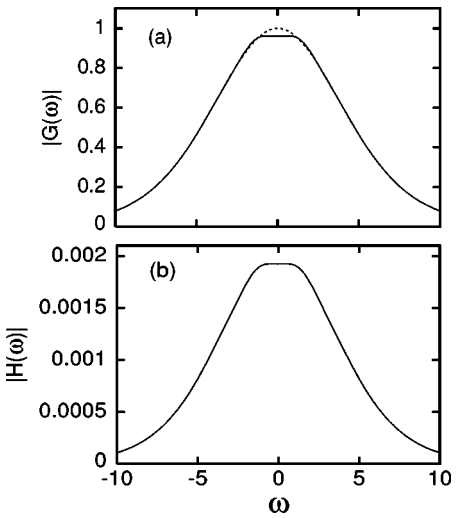

FIG. 4. Transfer functions characterizing the linear response of the Brillouin fiber amplifier in the weak saturation regime. The function $|G_0(\omega)|$ plotted by the dashed line is shown for reference. The parameters used are $g=10.98$, $\beta_A=18.22$, $I_p(0)=1$, $r=2\times10^{-3}$.

Increasing r to a numerical value of 2×10^{-3} first leads to a weak gain saturation. This is illustrated in Fig. 4(a) which shows that the function $|G(\omega)|$ deviates from the simple exponential form presented in Fig. 3(a). It flattens out and saturates to a constant value of 0.96 at low frequencies. This value is simply found to be the ratio between the saturated gain $\exp(\gamma)$ and the unsaturated gain $\exp[2gI_p(0)]$. The function $|H(\omega)|$ presents a shape that is comparable to that of $|G(\omega)|$ [see Fig. 4(b)]. However, its peak value that remains of the order of r has now increased to $\approx1.9\times10^{-3}$. As shown in Fig. 5(a), further increase in the parameter r leads to the emergence of a dip in the gain profile $|G(\omega)|$. For $r=0.01$, the central value of the gain $|G(0)|$ has fallen to 0.824. This value remains close to the ratio between the saturated and the unsaturated gain, which is equal to 0.802. As shown in Fig. 5(b), the shape of the transfer function $|H(\omega)|$ is comparable to that of $|G(\omega)|$ but it should be noticed that its peak value has further increased to a value of ≈0.0095. Summarizing our results, the central value of the gain $|G(0)|$ is approximately the ratio between the saturated and the unsaturated gain. Increasing r leads to a decrease of $|G(0)|$ and to an increase of the weight taken by the transfer function $|H(\omega)|$ whose peak value is always close to r. Therefore the emergence of spectral gain hole burning in the Brillouin fiber amplifier is due both to the gain saturation and to the coupling between the signal and pump perturbations. Gain saturation induces a flattening of the transfer function $|G(\omega)|$ but the intensity of the signal wave is so high then that the coupling between the signal and pump perturbations cannot be neglected. Contrary to the weak-interaction regime, the perturbation applied to the signal at $\zeta=1$ is not only carried by the signal wave but is also seen by the pump wave. For a particular frequency range, the coupling strength between the signal and pump perturbations is maximum and the two perturbations reinforce each other. This results in an increase of the gain $|G(\omega)|$ in spectral domains that are symmetrically placed around $\omega=0$. Therefore, the emergence of a dip in the gain profile can be seen rather as the growth of sidebands than as the birth of a spectral hole.

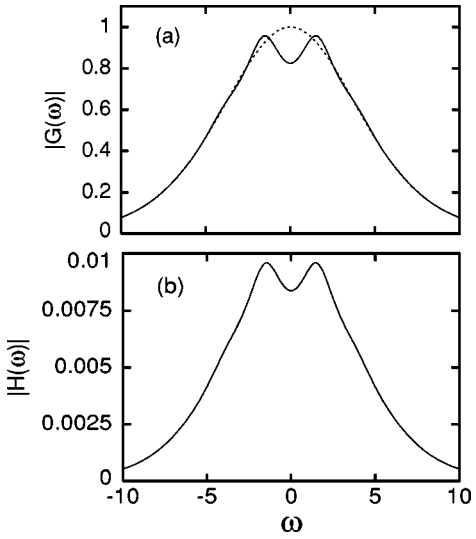

FIG. 5. Same as Fig. 4, but with $r=10^{-2}$.

D. Strong saturation regime

For values of the parameter r ranging approximately between 10^{-2} and 1, the Brillouin fiber amplifier operates in the strong saturation regime in which pump depletion cannot be ignored. The set of Eqs. (8) has been analytically solved by Fotiadi *et al.* in Ref. [22] for situations in which pump depletion is especially pronounced (i.e., for $r\simeq1$). As shown in detail in Appendix B, Eqs. (8) can also be analytically solved in the strong saturation regime for values of r ranging approximately between 10^{-2} and 0.1. The simplified analytical expressions of the stationary intensity profiles given by Eqs. (11b) and (12) are thus used and the set of Eqs. (8) is transformed into a second-order differential equation. Contrary to the weak saturation regime, the solution of this equation is no longer a sum of Bessel functions but of Whittaker functions [see Eq. (B4)] [21]. As shown in Fig. 6 obtained for $r=0.1$, the transfer functions $|G(\omega)|$ and $|H(\omega)|$ that are determined from the analytical solution [Eqs. (B6) and (B8)] exhibit a dip that is much deeper than that in the weak-interaction regime. Moreover, the two transfer functions are of the same order of magnitude and both of them exhibit a multipeak structure. Let us note that the validity of the analytical solution given in Appendix B has been tested by numerically integrating Eqs. (6) and (7). The relative difference between the analytical and the numerical solutions is lower than 1% as long as r does not exceed 0.1. For values of r greater than 0.1, the stationary intensity profiles can no longer be approximated by Eqs. (11b) and (12) so that the quantitative disagreement between the analytical and numerical solutions becomes significant. In very saturated amplification regimes, numerical simulations must, therefore, be used to characterize the linear response of the amplifier. The

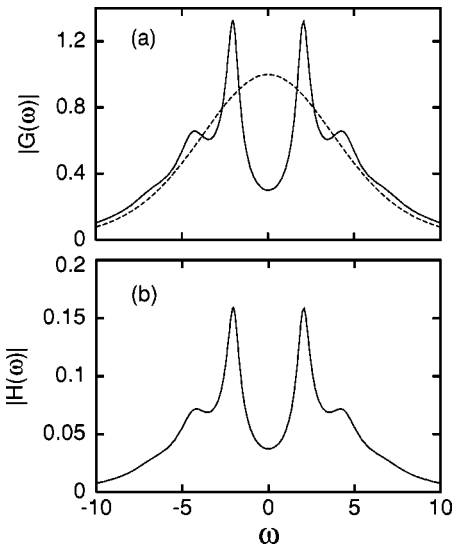

FIG. 6. Transfer functions characterizing the linear response of the Brillouin fiber amplifier in the strong saturation regime. The function $|G_0(\omega)|$ plotted by the dashed line is shown for reference. The parameters used are $g=10.98$, $\beta_A=18.22$, $I_p(0)=1$, $r=0.1$.

transfer functions that are plotted in Fig. 7 for $r=0.5$ have thus been numerically computed.

For $\omega>0$, Figs. 6 and 7 show that the angular frequency difference $\Delta\omega$ between two consecutive peaks of a given transfer function is approximately equal to π. Actually, it is worth noticing that similar features would be qualitatively observed in an empty Fabry-Perot cavity with the same length as our fiber. In such a resonator, a forward- and a backward-propagating wave are coupled by reflective boundary conditions at the right- and left-hand mirrors [23]. This results in the emergence of resonances separated by a normalized angular frequency equal to π. Let us now explain why a similar frequency difference appears in the Brillouin fiber amplifier, even though there is no mirror at the boundaries. This feature only arises from the fact that two coupled perturbations obeying well-defined boundary conditions counterpropagate in the amplifier. In the strong saturation regime, the pump and signal perturbations propagating around the stationary intensity profiles are of the same order of magnitude. These counterpropagating perturbations are coupled by the SBS interaction [see Eqs. (6a) and (6b)] and they must obey precise boundary conditions given by Eqs. (7). The combination of wave counterpropagation, SBS coupling, and boundary conditions is sufficient to give rise to resonances separated by an angular frequency difference approximately equal to π. This is shown in Appendix C in which very rough approximations are performed to simplify the problem and to show that the considered effect is only due to the presence of the three ingredients previously mentioned.

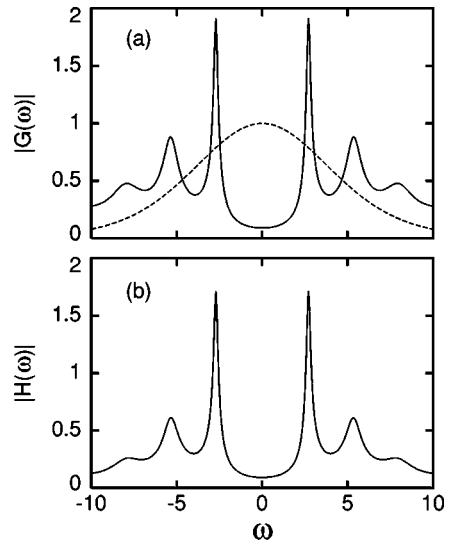

FIG. 7. Same as Fig. 6 but with $r=0.5$. Contrary to all the figures previously presented, the plotted transfer functions are obtained from numerical simulations (see the text).

It should be noticed that it is very difficult to avoid feedback from the boundaries in an optical-fiber medium. It is, furthermore, well established that the presence of weak Fresnel reflections at the fiber ends gives rise to periodic self-oscillations of the Stokes intensity [5,28,29]. In such a configuration, the system is no longer a simple amplifier but is termed a Brillouin fiber laser. The period of the observed steady oscillations is twice the transit time of the light in the fiber. In other words, the normalized angular frequency characteristic of the Stokes self-oscillations is equal to π when the SBS medium is enclosed within a Fabry-Perot cavity. It should be emphasized that these fluctuations of the Stokes intensity are not weak but result from oscillations on a limit cycle. Although their fundamental frequency can be found by a linear stability analysis [28,30], these self-oscillations involve the nonlinear response of the Brillouin fiber laser. On the other hand, the transfer functions considered in the present section characterize the linear response of the amplifier for a weak modulation of the signal amplitude. The same frequency found both in the laser and in the amplifier, therefore, characterizes responses and regimes that are fully different. On one hand, it represents the fundamental frequency of self-oscillations occurring in the nonlinear regime and on the other hand, it appears in a linear response to a weak modulation.

IV. SPECTRAL HOLE BURNING IN BRILLOUIN FIBER GENERATORS

In this section, we study theoretically the mechanisms leading to the emergence of hole burning in the spectrum of intensity fluctuations of the Stokes light emitted by Brillouin fiber generators. In particular, we will put emphasis on the connection between this phenomenon and the spectral hole burning already studied in Sec. III for Brillouin fiber amplifiers. The pump field being now the only external field injected inside the fiber, the only boundary condition that is taken into account is given by Eq. (2a). The weak noise term $f(\zeta,\tau)$ of Eq. (1c) describes the thermal excitation of acoustic waves. In the Brillouin fiber generator, it is responsible not only for the initiation of the SBS process, but also for the existence of a stochastic dynamics [3]. Contrary to Sec. III,

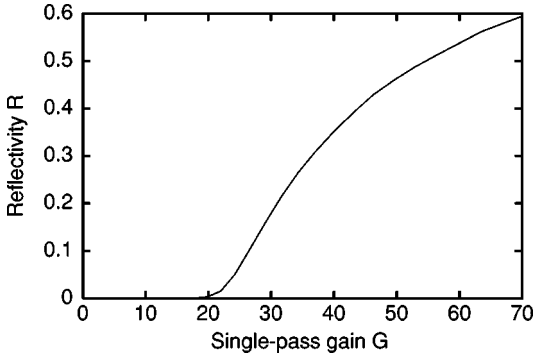

FIG. 8. Dependence of the reflectivity of a Brillouin fiber generator on the single-pass gain G_F ($g=10.98$, $\beta_A=18.22$).

its influence is now fully taken into account. The noise source $f(\zeta,\tau)$ being spatially distributed, the noise dominated SBS dynamics can only be studied by numerical simulations that have been performed by integrating the set of Eqs. (1) with a procedure based on the method of characteristics [23,24]. In order to unambiguously connect our numerical results to previous works performed on Brillouin fiber generators, we have chosen to use the parameters commonly employed to describe the power transfer characteristics of SBS generators. The first of these parameters is the reflectivity R defined as the ratio between the average output Stokes power and the incident pump power [$R=\langle|\varepsilon_s(\zeta=0,\tau)|^2\rangle/\mu^2$]. The other relevant parameter is the single-pass gain G_F defined as the product between the SBS gain factor measured in m/W, the pump laser intensity, and the fiber length [1]. With our normalization, it is also simply given by $G_F=2g\mu^2$. As shown in Fig. 8, the dependence of the SBS reflectivity on the single-pass gain G_F obtained from our numerical simulations is identical to that usually found in the SBS literature [2,3]. We especially underline this point since Kovalev and Harrison mention in Ref. [25] that ''our numerical modeling of SBS (presented in Ref. [10]) gives results which are intrinsically inconsistent and contradictory to the physics and practice of SBS.'' They also find in Ref. [25] many contradictions in the numerical results presented in our Comment [10] to their original Letter [9]; detailed numerical results supplementing those already published in Ref. [10] are presented hereafter. By using the parameters commonly employed to describe the physics of Brillouin fiber generators and by clearly specifying their numerical values, we hope to definitely clarify the situation and to conclusively demonstrate the consistency of our numerical simulations. Finally, the power spectra of the Stokes intensity fluctuations given hereafter are also presented in order to be directly compared to the transfer functions determined in Sec. III.

In Sec. III A, we have pointed out an analogy between pump-probe experiments in atomic systems and the three-wave configuration proposed by Takushima and Kikuchi to study the Brillouin fiber amplifier [see Fig. 1(b)]. A similar analogy can be drawn between fluorescence experiments in two-level atoms and studies performed in Brillouin fiber generators. In both cases, only one pump beam is injected inside the medium. In the Brillouin fiber generator, the backscattered Stokes light exhibits intensity fluctuations of a stochastic nature [3,5]. In two-level atomic systems, intensity fluctuations are observed in the emitted fluorescence [26]. In particular, it has been shown that the phase noise of the pump laser strongly affects the fluorescence intensity and the fluctuations of the fluorescence intensity [27]. Our numerical simulations have also shown that the Brillouin generator is sensitive to the phase noise of the pump laser. The SBS threshold is thus found to be dependent on the pump-laser linewidth. However, the effects described below remain qualitatively unchanged with or without the presence of pump phase noise.

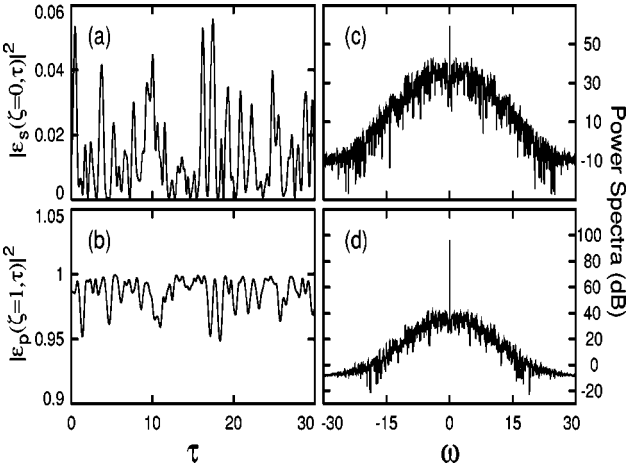

FIG. 9. Dynamical behavior of a Brillouin fiber generator operating close above threshold ($G_F=22$,$g=10.98$,$\beta_A=18.22$). Time series of the Stokes intensity at $\zeta=0$ (a) and corresponding power spectrum (c). Time series of the pump intensity at $\zeta=1$ (b) and corresponding power spectrum (d).

For a value of the single-pass gain close above the SBS threshold ($G_F=22$), the time evolutions of the Stokes and pump intensities are plotted in Figs. 9(a) and 9(b), respectively. The power spectra corresponding to these time series are presented in Figs. 9(c) and 9(d). Let us emphasize that the temporal signals presented in Fig. 9 are obtained after an integration time that is long enough to ensure that the system evolution takes place well after any transient process associated with the turn on of the pump laser. As shown in Fig. 9(a), the fluctuations in the Stokes intensity obtained from our numerical simulations are very similar to those reported by Boyd *et al.* in Ref. [3]. Despite the weak reflectivity ($R\simeq 1\%$), it should be noticed that the pump field at the output end of the fiber ($\zeta=1$) exhibits weak intensity fluctuations around a strong dc background [see Fig. 9(b)]. The power spectrum of this signal is thus composed of a strong dc component that is approximately ≈ 50 dB above the noise level [see Fig. 9(d)]. As shown in Fig. 9(c), the power spectrum of the Stokes intensity fluctuations is qualitatively similar to the power spectrum of the pump intensity fluctuations. The only significant difference lies in the weight of the dc component that is only 20 dB above the noise level. Figure 10 shows the time series and power spectra obtained well above the SBS threshold for $G_F=60$. The reflectivity is now $\approx 50\%$ and the intensity of the pump and Stokes fields is strongly fluctuat-

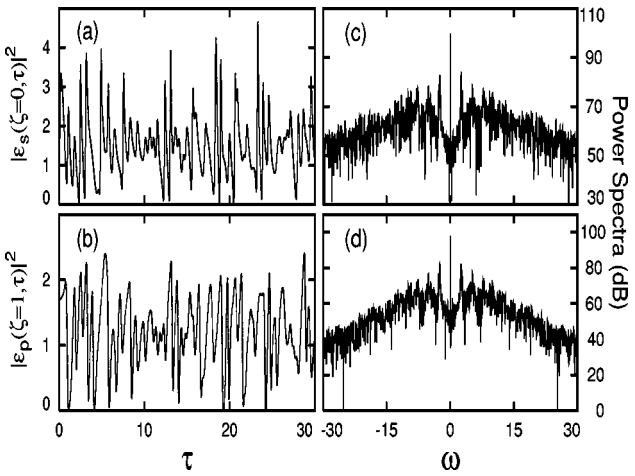

FIG. 10. Same as Fig. 9 but well above threshold ($G_F=60$).

ing. The power spectra are very different from those of Fig. 9. As in the experiments of Ref. [9], both of them now exhibit a pronounced dip around $\omega=0$. Moreover, a careful analysis of Figs. 10(c) and 10(d) reveals several peaks that are symmetrically and regularly spaced around $\omega=0$. This strongly suggests to compare the power spectra of Fig. 10 with the transfer functions presented in Fig. 7. To this end, we rescale the function $|G(\omega)|$ by plotting the function $G_{dB}(\omega)=20\log_{10}|G(\omega)|$ which permits a direct comparison between power spectra and transfer functions. Figure 11(b) thus shows that the power spectrum of Fig. 10(c) obtained for $R=50\%$ is very similar to the transfer function of Fig. 7(a) computed for a ratio $r=I_s(0)/I_p(0)$ of 0.5. Let us notice that the spectrum presented in Fig. 11(b) has been obtained by averaging the power spectra of Stokes intensity

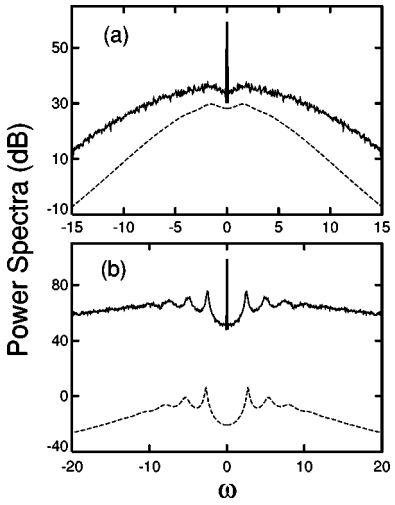

FIG. 11. Comparison between the power spectra of Stokes intensity fluctuations in the Brillouin fiber generator (full lines) and the transfer functions $G_{dB}(\omega)$ of the Brillouin fiber amplifier (dashed lines). (a) Weak reflectivity ($R\simeq 1\%$, $G_F=22$) and weak saturation regime ($r=0.01$). (b) Strong reflectivity ($R\simeq 50\%$, $G_F=60$) and strong saturation regime ($r=0.5$). Note that an arbitrary offset of 30 dB has been added to the transfer function of (a) in order to permit a direct comparison between the two small dips.

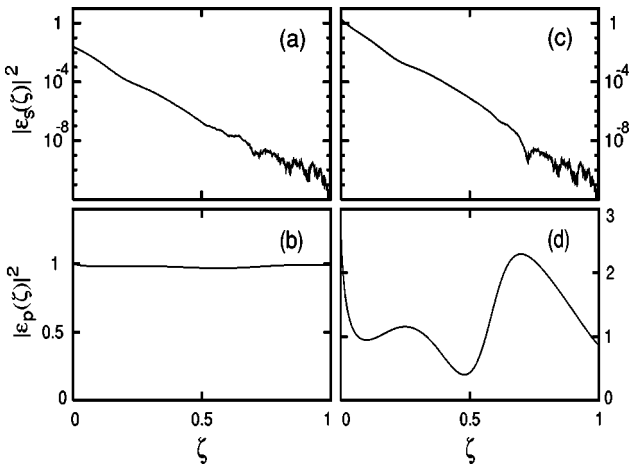

FIG. 12. Longitudinal profiles of the Stokes (a),(c) and pump (b),(d) intensities at an arbitrary time for gain factors G_F of 22 (a),(b) and 60 (c),(d).

fluctuations over 100 realizations of the random process $f(\zeta,\tau)$. This averaging procedure permits to remove almost all the noise that superimposes on the spectrum of Fig. 10(c). This is also especially useful for noise spectra computed for weak reflectivities. Figure 11(a) indeed reveals a small dip in the power spectrum obtained for a reflectivity of 1%. As shown in Fig. 9(c), it is not observable in only one spectrum. However, it is very similar to the dip characterizing the transfer function $G_{dB}(\omega)$ that has been computed for a Brillouin fiber amplifier operating in the weak saturation regime for $r=I_s(0)/I_p(0)=0.01$.

Let us now summarize our results and discuss their significance. In a Brillouin fiber generator reflecting a given percentage R of the incident pump intensity, the power spectrum of the Stokes intensity fluctuations is very similar to the transfer function characterizing the linear response of a Brillouin fiber amplifier operating in such a way that $r=I_s(0)/I_p(0)$ is equal to R. Rigorously speaking, the transfer functions considered in Sec. III properly characterize the intensity noise properties of a Brillouin amplifier operating in the configuration represented in Fig. 1(a). Instead of a weak intensity modulation applied at the output end of the fiber (see Fig. 2), a weak noise source must obviously be added to the signal wave at $\zeta=1$. The spectral density of signal intensity noise at $\zeta=0$ is then simply obtained by multiplying the spectral density of signal intensity noise at $\zeta=1$ by $|G(\omega)|^2$.

In a Brillouin fiber generator, the situation is not so simple. First of all, no signal wave is injected inside the fiber. This means that no stationary state can be rigorously defined. However for weak reflectivities, pump depletion can be neglected and the Stokes light is exponentially amplified on the average as it propagates inside the fiber [2]. This is illustrated in Figs. 12(a) and 12(b), which show the Stokes and pump intensity profiles at an arbitrary time. The term $f(\zeta,\tau)$ induces weak fluctuations around the exponential Stokes intensity profile [see Fig. 12(a)] but the reflectivity is so small that the pump intensity profile is not significantly perturbated [see Fig. 12(b)]. Contrary to the situation previously de-

scribed for the Brillouin fiber amplifier, the origin of the weak fluctuations is not a localized noise source but a spatially distributed noise source. Nevertheless, we can apply arguments identical to those previously used for the discussion of noise properties of Brillouin fiber amplifiers. The weak fluctuations around the exponential intensity profile characterizing the average amplification of the Stokes wave are filtered by the transfer function $|G(\omega)|$ studied in Sec. III C. This results in a noise power spectrum at $\zeta=0$, which is very similar to the transfer function of the amplifier.

For higher reflectivities, the coupling between the Stokes and pump fluctuations becomes significant. This is illustrated in Figs. 12(c) and 12(d), which show that the Stokes field is now so intense that its fluctuations induce strong variations of the pump intensity profile. The coupled pump and Stokes perturbations counterpropagate around mean intensity profiles that are determined by the reflectivity. The situation can thus be compared to that studied in Sec. III D for a Brillouin fiber amplifier operating in the strong saturation regime. Despite the fact that the intensity fluctuations are now stronger, the analysis previously developed for the weak reflectivity regime still qualitatively holds for the strong reflectivity regime. The Stokes intensity fluctuations are filtered by the transfer function $|G(\omega)|$ numerically computed in Sec. III D for a Brillouin fiber amplifier operating in the strong saturation regime. This results in a dip in the power spectrum of Stokes intensity fluctuations and in the emergence of peaks arising from the counterpropagation and the coupling between pump and Stokes fluctuations inside the generator.

V. CONCLUSION

In summary, spectral hole burning in Brillouin fiber amplifiers and generators has been theoretically studied. Transfer functions characterizing the linear response of the Brillouin amplifier to a weak amplitude modulation of the injected signal wave have been analytically determined for three different amplification regimes. The fact that these transfer functions may exhibit a dip is due both to the gain saturation and the coupling between the pump and signal perturbations that counterpropagate around the steady-state intensity profiles. The transfer functions also relate the intensity noise of the amplified signal wave to the intensity noise of the injected signal wave. In other words, they characterize the way through which a weak noisy perturbation propagating around the stationary intensity profiles is filtered by the Brillouin fiber amplifier. In the Brillouin fiber generator, one cannot consider that the Stokes intensity fluctuates around a well-defined stationary profile, but around a mean spatial profile determined by the reflectivity. Nevertheless, the Stokes intensity fluctuations are filtered in the same way as signal intensity fluctuations in a Brillouin fiber amplifier. This results in a dip in the power spectrum of the Stokes intensity noise.

Our interpretation of spectral hole burning in Brillouin fiber generators is very different from the interpretation proposed by Kovalev and Harrison in Ref. [9]. In particular, we have shown that this effect can be understood without invoking an inhomogeneous broadening of the Brillouin line. However, one significant qualitative difference between theoretical and experimental results must be underlined. The power spectra of Stokes intensity fluctuations obtained from our numerical simulations [see our Fig. 10(c) and Fig. 1 of Ref. [10]] show evidence of peaks regularly spaced that are not found in the experiments (see Fig. 1 of Ref. [9]). Following our interpretation, these peaks are a signature of the interaction between the counterpropagating pump and signal fluctuations. In our opinion, the fact that they are not observed in the experiments may be due either to their weakness or to a poor instrumental resolution. Another way to experimentally check the existence of coupling between Stokes and pump intensity fluctuations would simply consist in putting a photodiode at the output end of the fiber in order to monitor the time evolution of the transmitted pump intensity. The observation of a dip in the power spectrum of pump intensity fluctuations would then indisputably validate our interpretation of spectral hole burning in Brillouin fiber generators.

ACKNOWLEDGMENTS

The Centre d'Etudes et de Recherches Lasers et Applications (CERLA) is supported by the Ministère Chargé de la Recherche, the Région Nord/Pas de Calais, and the Fonds Européen de Développement Economique des Régions. This work was partially supported by the European contract ''Intereg II Nord-Pas de Calais/Kent.''

APPENDIX A: ANALYTICAL DETERMINATION OF THE TRANSFER FUNCTIONS $|G(\omega)|$ AND $|H(\omega)|$ IN THE WEAK SATURATION REGIME

Combining Eq. (7a) with Eq. (8a) permits one to obtain a condition for $\widetilde{\delta A}_s(u,\omega)$ that reads

$$\left.\frac{\partial\widetilde{\delta A}_s(u,\omega)}{\partial u}\right|_{u=1} = D\widetilde{\delta A}_s(u=1,\omega) \tag{A1}$$

with $D=-i\Omega_0^2/(\gamma\omega)$. From this condition and by using Eq. (23), we obtain

$$|G(\omega)| = \left|\frac{[PJ_A(B)+QY_A(B)]\exp(\Gamma_0)}{PJ_A(Be^{-\gamma/2})+QY_A(Be^{-\gamma/2})}\right| \tag{A2}$$

with

$$P = BY_{A+1}(B) - NY_A(B), \tag{A3a}$$

$$Q = -BJ_{A+1}(B) + NJ_A(B), \tag{A3b}$$

$$N = A + \frac{2\Gamma_0}{\gamma} - 2D. \tag{A3c}$$

The analytical expression of $|H(\omega)|$ derived from Eqs. (8a) and (23) reads

$$|H(\omega)| = \left|\frac{T(PS_J+QS_Y)}{PJ_A(Be^{-\gamma/2})+QY_A(Be^{-\gamma/2})}\right| \tag{A4}$$

with

$$S_J = -Be^{-\gamma/2}J_{A+1}(Be^{-\gamma/2}) + NJ_A(Be^{-\gamma/2}), \quad \text{(A5a)}$$

$$S_Y = -Be^{-\gamma/2}Y_{A+1}(Be^{-\gamma/2}) + NY_A(Be^{-\gamma/2}), \quad \text{(A5b)}$$

$$T = \frac{\gamma}{2gI_p(0)\left(1+\frac{\beta_A}{\beta_A+i\omega}\right)}. \quad \text{(A5c)}$$

APPENDIX B: ANALYTICAL DETERMINATION OF THE TRANSFER FUNCTIONS $|G(\omega)|$ AND $|H(\omega)|$ IN THE STRONG SATURATION REGIME

By using Eqs. (11b) and (12), the set of Eqs. (8) is transformed into a second-order differential equation that reads

$$\frac{\partial^2\widetilde{\delta A}_s(\zeta,\omega)}{\partial\zeta^2} + 2(\Delta_0+\Delta_1 e^{-\gamma\zeta})\frac{\partial\widetilde{\delta A}_s(\zeta,\omega)}{\partial\zeta} + (\Theta_0^2+\Theta_1^2 e^{-\gamma\zeta})\widetilde{\delta A}_s(\zeta,\omega) = 0 \quad \text{(B1)}$$

with

$$\Delta_0 = \frac{-i\omega\gamma}{4(\beta_A+i\omega)}, \quad \Delta_1 = \frac{g\beta_A r I_p(0)}{\beta_A+i\omega}, \quad \text{(B2a)}$$

$$\Theta_0 = \omega^2\left(1+\frac{\gamma}{2(\beta_A+i\omega)}\right),$$

and

$$\Theta_1 = -2grI_p(0)\left(i\omega+\frac{2\beta_A g I_p(0)}{\beta_A+i\omega}\right). \quad \text{(B2b)}$$

As already achieved in Sec. III C, we introduce the new variable $u=\exp(-\gamma\zeta)$, and Eq. (B1) becomes

$$\gamma^2u^2\frac{\partial^2\widetilde{\delta A}_s(u,\omega)}{\partial u^2} + \gamma u(\gamma-2\Delta_0-2\Delta_1 u)\frac{\partial\widetilde{\delta A}_s(u,\omega)}{\partial u} + (\Theta_0^2+\Theta_1^2 u)\widetilde{\delta A}_s(u,\omega) = 0. \quad \text{(B3)}$$

The solution of this equation is a sum of Whittaker functions $M_{\eta,\kappa}(\chi u)$ and $W_{\eta,\kappa}(\chi u)$ defined in Ref. [21]. It reads

$$\widetilde{\delta A}_s(u,\omega) = [C_1'' M_{\eta,\kappa}(\chi u) + C_2'' W_{\eta,\kappa}(\chi u)]\exp\left(\frac{\chi u}{2}\right)u^\rho \quad \text{(B4)}$$

with

$$\eta = \frac{\Theta_1^2+\gamma\Delta_1-2\Delta_0\Delta_1}{2\gamma\Delta_1}, \quad \kappa = \frac{\sqrt{\Delta_0^2-\Theta_0^2}}{\gamma},$$

$$\chi = \frac{2\Delta_1}{\gamma}, \quad \text{and} \quad \rho = \frac{-\gamma+2\Delta_0}{2\gamma}. \quad \text{(B5)}$$

By determining the ratio between the integration constants C_1'' and C_2'' from Eq. (A1), we finally obtain the following analytical expression for the transfer function $|G(\omega)|$ in the strong saturation regime:

$$|G(\omega)| = \left|\frac{[P'M_{\eta,\kappa}(\chi)+Q'W_{\eta,\kappa}(\chi)]\exp\left[\frac{\chi}{2}(1-e^{-\gamma})+\gamma\rho\right]}{P'M_{\eta,\kappa}(\chi e^{-\gamma})+Q'W_{\eta,\kappa}(\chi e^{-\gamma})}\right| \quad \text{(B6)}$$

with

$$P' = 2W_{\eta+1,\kappa}(\chi)+N'W_{\eta,\kappa}(\chi), \quad \text{(B7a)}$$

$$Q' = (1+2\eta+2\kappa)M_{\eta+1,\kappa}(\chi)-N'M_{\eta,\kappa}(\chi), \quad \text{(B7b)}$$

$$N' = 2(\eta-\chi-\rho+D). \quad \text{(B7c)}$$

The analytical expression of $|H(\omega)|$ derived from Eqs. (8a) and (B4) reads

$$|H(\omega)| = \left|\frac{T'(P'S_M+Q'S_W)}{P'M_{\eta,\kappa}(\chi e^{-\gamma})+Q'W_{\eta,\kappa}(\chi e^{-\gamma})}\right| \quad \text{(B8)}$$

with

$$S_M = \Lambda M_{\eta,\kappa}(\chi e^{-\gamma}) + \left(\frac{1}{2}+\eta+\kappa\right)M_{\eta+1,\kappa}(\chi e^{-\gamma}), \quad \text{(B9a)}$$

$$S_W = \Lambda W_{\eta,\kappa}(\chi e^{-\gamma}) - W_{\eta+1,\kappa}(\chi e^{-\gamma}), \quad \text{(B9b)}$$

$$\Lambda = \chi e^{-\gamma}+\rho-\eta+\frac{i\omega}{\gamma}\left(\frac{gI_p(0)[1-r(1-e^{-\gamma})]}{\beta_A+i\omega}+1\right), \quad \text{(B9c)}$$

$$T' = \frac{\gamma}{gI_p(0)[1-r(1-e^{-\gamma})]\left(1+\frac{\beta_A}{\beta_A+i\omega}\right)}. \quad \text{(B9d)}$$

APPENDIX C: SIMPLIFIED ANALYSIS OF THE ORIGIN OF THE RESONANCE FREQUENCIES APPEARING IN THE TRANSFER FUNCTIONS

In this appendix, we perform a very simplified analytical treatment to show that only three elementary ingredients are necessary to explain the emergence of a normalized angular frequency difference of approximately π in the transfer functions characterizing the response of the amplifier. These ingredients are counterpropagation of pump and signal perturbations around arbitrary stationary intensity profiles, SBS coupling, and boundary conditions for the perturbations at the ends of the fiber. We first assume an instantaneous acoustic response, so that the set of Eqs. (6) reduces to

$$\frac{\partial \widetilde{\delta A}_p}{\partial \tau} + \frac{\partial \widetilde{\delta A}_p}{\partial \zeta} = -2gI_s(\zeta)\widetilde{\delta A}_s, \tag{C1a}$$

$$\frac{\partial \widetilde{\delta A}_s}{\partial \tau} - \frac{\partial \widetilde{\delta A}_s}{\partial \zeta} = 2gI_p(\zeta)\widetilde{\delta A}_p. \tag{C1b}$$

By taking the Fourier transform of Eqs. (C1), we obtain the following second-order differential equation:

$$\frac{\partial^2 \widetilde{\delta A}_s(\zeta,\omega)}{\partial \zeta^2} + \Omega^2 \widetilde{\delta A}_s(\zeta,\omega) = 0 \tag{C2}$$

with

$$\Omega^2 = \omega^2 - 4g^2 I_p(\zeta) I_s(\zeta). \tag{C3}$$

The existence of stationary intensity profiles around which the propagation of the pump and signal perturbations is possible is obviously crucial, but their shape is not critical in order to explain the emergence of resonance frequencies. Although it is not physically realistic, we will, therefore, assume that the stationary intensity profiles do not depend on ζ. The solution of Eq. (C2) is then trivial and reads

$$\widetilde{\delta A}_s(\zeta,\omega) = C_1 \exp(i\Omega\zeta) + C_2 \exp(-i\Omega\zeta). \tag{C4}$$

We will now reduce our analysis to situations for which ω^2 is greater than $4g^2 I_p I_s$, so that Ω is real. This amounts to only considering situations in which $\widetilde{\delta A}_s(\zeta,\tau)$ is the sum of a forward- and a backward-propagating sine wave. The transfer function $|G(\omega)|$ relating the amplitude fluctuations of the signal at $\zeta=0$ to the amplitude fluctuations of the signal applied at $\zeta=1$ is obtained by using the boundary condition given by Eq. (7a). It simply reads

$$|G(\omega)|^2 = \left| \frac{\widetilde{\delta A}_s(\zeta=0,\omega)}{\widetilde{\delta A}_s(\zeta=1,\omega)} \right|^2 = \frac{(1+a)^2}{1+a^2+2a\cos(2\Omega)} \tag{C5}$$

with

$$a = \frac{\Omega-\omega}{\Omega+\omega}, \quad \Omega = \omega\sqrt{1-\frac{4g^2 I_p I_s}{\omega^2}}. \tag{C6}$$

The expression given by Eq. (C5) is very similar to the transmission function characterizing an empty Fabry-Perot cavity [23]. In particular, resonances are obtained each time Ω rotates by π. The corresponding rotations of the normalized angular frequency ω are equal to π if $\omega^2 \gg 4g^2 I_p I_s$, and they are slightly lower than π if $\omega^2 \simeq 4g^2 I_p I_s$.

[1] G. P.;Agrawal, *Nonlinear Fiber Optics* (Academic, New York, 1989).
[2] R. W. Boyd, *Nonlinear Optics* (Academic, San Diego, 1992).
[3] R.W. Boyd, K. Rzażewski, and P. Narum, Phys. Rev. A **42**, 5514 (1990).
[4] A.L. Gaeta and R.W. Boyd, Phys. Rev. A **44**, 3205 (1991).
[5] M. Dämmig, G. Zinner, F. Mitschke, and H. Welling, Phys. Rev. A **48**, 3301 (1993).
[6] M. Niklès, L. Thévenaz, and P.A. Robert, J. Lightwave Technol. **LT15**, 1842 (1997).
[7] A. Yariv, *Quantum Electronics*, 3rd ed. (Wiley, New York, 1988).
[8] Y. Takushima and K. Kikuchi, in *1999 IEEE LEOS Annual Meeting Conference Proceedings*, IEEE Laser and Electro-Optics Society 1999 Annual Meeting (IEEE, Piscataway, NJ, 1999), Vol. 1, p. 58.
[9] V.I. Kovalev and R.G. Harrison, Phys. Rev. Lett. **85**, 1879 (2000).
[10] S. Randoux and J. Zemmouri, Phys. Rev. Lett. **88**, 029401 (2002).
[11] A.A. Fotiadi, R. Kiyan, O. Deparis, P. Mégret, and M. Blondel, Opt. Lett. **27**, 83 (2002).
[12] Y. Takushima and K. Kikuchi, Opt. Lett. **20**, 34 (1995).
[13] C. Montes, A. Mamhoud, and E. Picholle, Phys. Rev. A **49**, 1344 (1994).
[14] C.C. Chow and A. Bers, Phys. Rev. A **47**, 5144 (1993).
[15] W. Lu, A. Johnstone, and R.G. Harrison, Phys. Rev. A **46**, 4114 (1992).
[16] J. Botineau, C. Leycuras, C. Montes, and E. Picholle, Ann. Telecommun. **49**, 479 (1994).
[17] J. Botineau, C. Leycuras, C. Montes, and E. Picholle, J. Opt. Soc. Am. B **6**, 300 (1989).
[18] S.E. Schwarz and T.Y. Tan, Appl. Phys. Lett. **10**, 4 (1967).
[19] L.W. Hillman, R.W. Boyd, J. Krasinski, and C.R. Stroud, Opt. Commun. **45**, 416 (1983).
[20] R.W. Boyd and S. Mukamel, Phys. Rev. A **29**, 1973 (1984).
[21] *Handbook of Mathematical Functions* edited by M. Abramowitz and I. Stegun (Dover, New York, 1974).
[22] A.A. Fotiadi, E.A. Kuzin, M.P. Petrov, and A.A. Ganichev, Pis'ma Zh. Tekh. Fiz. **15**, 48 (1989) [Sov. Tech. Phys. Lett. **15**, 434 (1989)].
[23] A. C. Newell and J. V. Moloney, *Nonlinear Optics* (Addison-Wesley, Redwood City, CA, 1992).
[24] V. Babin, A. Mocofanescu, V.I. Vlad, and M.J. Damzen, J. Opt. Soc. Am. B **16**, 155 (1999).
[25] V.I. Kovalev and R.G. Harrison, Phys. Rev. Lett. **88**, 029402 (2002).
[26] M.H. Anderson, R.D. Jones, J. Cooper, S.J. Smith, D.S. Elliott, H. Ritsch, and P. Zoller, Phys. Rev. Lett. **64**, 1346 (1990).
[27] H. Ritsch, P. Zoller, and J. Cooper, Phys. Rev. A **41**, 2653 (1990).
[28] I. Bar-Joseph, A.A. Friesem, E. Lichtman, and R.G. Waarts, J. Opt. Soc. Am. B **2**, 1606 (1985).
[29] A.L. Gaeta and R.W. Boyd, Int. J. Nonlinear Opt. Phys. **1**, 581 (1992).
[30] R. Blaha, E.W. Laedke, A.M. Rubenchik, and K.H. Spatschek, Europhys. Lett. **7**, 237 (1988).